University of Baghdad
College of Engineering
JOURNAL OF ENGINEERING

Journal of Engineering

journal homepage: www.jcoeng.edu.iq

Volume 32 Number 9 September 2026

Crown-Shaped Patch Antenna with CSRR and Nd:YAG Laser Surface Treatment for C-Band Communication

Rusull Kha. Rustum *, **Ali H. Khidhir**

Department of Physics, College of Science, University of Baghdad, Baghdad, Iraq

ABSTRACT

In this paper a compact four-port crown-shaped MIMO antenna is proposed for sub-6 GHz wireless applications and fabricated on FR4 substrate. The peak gain is 4.57 dBi, and the radiation efficiency is above 75% at wide impedance bandwidth of 4.0–4.8 GHz, with operation against about 4.5 GHz as expected. The crown geometry allows for improved impedance matching, better structural symmetry and lower mutual coupling when compared to conventional patch antennas. In order to increase practical performance, Nd:YAG laser surface treatment is used as a post-fabrication approach that decreases the RMS surface roughness from 385 nm to 78 nm in order to reach maximum electrical conductivity and minimum conductor losses. As a result, the reflection coefficient below −30 dB is measured, the VSWR reaches values close to unity and provides 50 Ω input impedance. The MIMO system in this case also shows an optimal diversity with ECC near idle (0.01) and a diversity gain of approximately 10 dB. Closer agreement between simulated and measured results, especially after laser treatment, has validated the design and demonstrated the ability of laser post-processing to decrease fabrication tolerances. The antenna is structurally unique in integrating a crown-shaped fractal patch geometry with the complement split-ring resonator, which breaks the surface current symmetry to excite orthogonal modes to realize a significantly wide impedance bandwidth across sub-6 GHz spectrum. This achieves natural decoupling through its inherent spatial diversity and orthogonal port orientations without complex but bulky decoupling networks crucial for the compact form factor needed in dense 5G terminals.

Keywords: 5G, MIMO antenna, Crown-shaped, Nd:YAG laser treating, ECC, DG.

1. INTRODUCTION

Microstrip patch antennas (MPAs) and multiple-input multiple-output (MIMO) systems are widely used in communications these days because of their compact size, low profile, cost-efficient, and easy implementation **(Hakeem and Nahas, 2021; Wong et al., 2002; Pozar, 2012).** Thus, their characteristics allow them to be very attractive candidates for new

*Corresponding author
Peer review under the responsibility of University of Baghdad.
https://doi.org/10.31026/j.eng.2026.09.09

Article received: 12/04/2026
Article revised: 10/08/2026
Article accepted: 15/08/2026
Article published: 01/09/2026

applications like fifth generation (5G) and beyond wireless systems that require unbounded data rates spectral efficiency and reliability. Despite the great progress, ensuring antenna performance at their best such as in-bandwidth, gain, radiation efficiency and mutual coupling suppression is still a vital design issue **(Biswas and Sarkar, 2020; Xu et al., 2020).** Various enhancement methods were introduced in the literature to tackle these issues. Electromagnetic band gap (EBG) structures and defected ground structures (DGS) have been used as an effective way to enhance impedance bandwidth and minimize mutual coupling of the antenna elements **(Yang and Rahmat-Samii, 2009; Singh and Kumar, 2021; Chahboun et al., 2024)**. These structures inhibit the propagation of surface waves while allowing more selective radiation characteristics. In addition, metamaterial-inspired structures including complementary split-ring resonators (CSRRs) have proven to be effective in improving the radiation characteristics, bandwidth performance and compactness of antenna designs **(Abbosh, 2013; Prashanth et al., 2023).** Meta-material elements can be integrated with such devices to develop unique electromagnetic characteristics that are not possible in conventional antennas.

Metallization of antenna polymer substrates has seen improvements with the advent of laser-based surface treatment strategies, including new approaches to post-fabrication optimization through Nd:YAG laser processing. Such methods not only increase gain but also frequency and radiation efficiency, as well as reduce surface roughness and mutual coupling **(Khoudair and Khidhir, 2025; Kareem et al., 2024).** Substrate antenna laser processing the laser processing method is a new non-contact electromagnetism surface treatment ability to improve many aspects of characteristics of substrate and conductor surfaces, which could have performance enhancement. Here, this drive for improved manufacturing answers to shortcomings in fabrication and out-of-tolerance components that are the root causes of a disconnect between simulation predictions and measurement results. Particularly, compact multiple-input multiple-output (MIMO) antennas have been widely deployed in contemporary wireless devices while relatively high efficiency using small size with low envelope correlation coefficient (ECC) is required for reliable wireless communication and maintaining diversity performance **(Asiegbu et al., 2024; Biswas and Sarkar, 2020).** The ECC metric is significant for MIMO system performance because it estimates the correlation between antenna elements and how efficient the implemented system gives spatial diversity. More advanced multi-port systems with enhanced diversity, isolation and data rates have recently been proposed to accommodate the severe requirements of 5G and beyond (6G) networks **(Baban and Al-Rasheed, 2026; Bellekhiri et al., 2024)**.

Other investigations on antenna types and feeding techniques (circular patch antennas, aperture-coupled designs, array based setups, crown shape structures) have aimed to better transfer radiation of the emitted signal leading towards a higher efficiency of this system **(Bhosale and Ghanshyam, 2025; Bellekhiri et al., 2024; Zhang et al., 2023).** The choice of patch geometry substantially modifies the resonant frequency, bandwidth and radiation characteristics of antenna. In addition, many ultra-wideband (UWB) and reconfigurable antennas have successfully exploited slot engineering and adaptive frameworks to further enhance the bandwidth with relatively high gain alongside commendable isolation characteristics. Design innovation that enables antennas to function effectively in multiple frequency bands simultaneously More specifically, at the millimeter-wave (mmWave) bands, it ranges from 28 GHz to 38 GHz and beyond where MIMO antennas featuring DGS paired with spatial diversity and hybrid coupling reduction techniques give very high values of gain, isolation and radiation efficiency. Recent methods such as using periodic structures, artificial magnetic conductors and meta surfaces have reduced mutual coupling even further with the advantage of high efficiency and small physical dimensions **(Karahan, 2025; Chahboun et al., 2024)**. For mmWave and sub-6 GHz bands a new combination of both high gain (9 dBi) but low MIMO envelope correlation coefficients (ECC < 0.001) suitable for deployment in next generation wireless systems was achieved. With the passage of years, mitigation techniques have evolved from simple stubs and filters to sophisticated decoupling networks as well as hybrid isolation structures **(Khan et al., 2020; Hussain et al., 2023; Munusami and Venkatesan, 2024)**. These methods reduce the impact of both near and far-field coupling mechanisms, enabling elements to be situated much closer together yet still meet acceptable isolation levels (greater than −20 dB in most cases). In this case, defected ground structures are especially efficient because they prevent the surface waves from propagating without requiring any additional area on the antenna substrate. Further, isolation improved in a few frequency bands have been realized through neutralization lines, parasitic elements and frequency selective surfaces **(Zhang and Pedersen, 2015; Dhasarathan et al., 2023).** Utilization of EBG and metamaterial structures in compact MIMO designs has demonstrated remarkable duality: not only does it enhance bandwidth but also isolates **(Elabd and Al-Gburi, 2024; Jemaludin et al., 2025)**. They have been used to control electromagnetic field localization through artificial bandgaps or dispersion property modification. CSRRs and SRRs form compact metamaterials that can be used to create antennas in small form-factor systems **(Dam et al., 2023).** The miniaturization permit through metamaterial loading also allows for antenna designs which are space restrictive as found in many forms of mobile electronics such as smart phone, tablets and wearables. However, despite all of these advances, it is nontrivial to design a compact MIMO antenna that achieves high efficiency (over 85%), low mutual coupling (below −25 dB), stable impedance matching over wide bands and great diversity performance at the same time. In addition, many of the published works do not adequately consider the differences between simulation and measurement results that commonly arise from fabrication imperfections, substrate tolerances, conductor losses etc. Surface roughness has been shown to impact antenna performance **(Žemgulytė et al., 2023; Kareem et al., 2024)**, but there are gaps in literature regarding antenna operation at higher frequencies where skin-effect losses become non-negligible.

To address this issue, a new Nd:YAG laser-assisted four-port crown-shaped MIMO antenna is designed in this paper. We propose laser ablation of the metallic surface: this procedure not only improves the surface properties but also reduces the surface roughness to submicrometer values, which significantly narrows the delta between simulated and experimental results. The crown-shaped geometry offers exclusive electromagnetic properties that improve radiation patterns and impedance matching. This can be achieved with laser post-processing that permits setting the antenna parameters together with its surface properties after fabrication and, thus, compensating for manufacturing tolerances while optimizing performance **(Khoudair and Khidhir, 2025; Kareem et al., 2024)**.

To address these identified gaps, this paper presents a compact four-port crown-shaped MIMO microstrip patch antenna fabricated on an FR4 substrate, incorporating complementary split-ring resonators for mutual coupling suppression. The antenna operates at approximately 4.5 GHz within the C-band sub-6 GHz range. Following fabrication, Nd:YAG laser surface polishing is applied to the copper conductive layer as a controlled post-fabrication treatment, reducing surface roughness from 385 nm to 78 nm

(Ra). The effect of this treatment on antenna RF performance is systematically characterized through comparison of pre- and post-treatment measurements. The specific contributions of this work are threefold: (1) a crown-shaped four-port MIMO antenna geometry that achieves improved impedance matching and reduced mutual coupling compared to conventional rectangular patch designs within the same footprint; (2) integration of CSRR structures within the ground plane to enhance inter-element isolation; and (3) experimental demonstration that controlled Nd:YAG laser surface polishing reduces conductor losses and measurably improves reflection coefficient, VSWR, and ECC in a fabricated MIMO antenna system.

2. MATERIALS AND METHODS

2.1 Geometry and Antenna Design

This section describes the theoretical formulation of the new four-port MIMO antenna array and design methodology. The transmission line model is used to calculate the initial physical measurements of the microstrip patch antenna at a specific resonant frequency (4.5 GHz) **(Aziz and Hasan, 2024).**

$$W = \frac{c}{2f_r}\sqrt{\frac{2}{\epsilon_r + 1}} \tag{1}$$

where c = 3 × 108 m/s denotes the speed of light in free space, f_r is the resonant frequency (4.5 GHz), and ε_r is the relative permittivity of the substrate material. In this design, an FR4 substrate with ε_r = 4.4 is employed.

Prior to calculating the fringing field extension, the effective dielectric constant ε_{reff} must be determined. For a microstrip line with patch width W and substrate thickness h, the effective dielectric constant is given by **(Aziz and Hasan, 2024)**:

$$\varepsilon_{reff} = \frac{(\varepsilon r + 1)}{2} + \frac{(\varepsilon r - 1)}{2} \times (1 + \frac{12h}{W})^{-\frac{1}{2}} \tag{2}$$

where h = 1.6 mm is the substrate thickness.

The incremental line extension ΔL) caused by the fringing effect is evaluated as

$$\Delta L = 0.412h \frac{(\epsilon_{reff} + 0.3)(\frac{W}{h} + 0.264)}{(\epsilon_{reff} \_ 0.582)(\frac{W}{h} + 0.8)} \tag{3}$$

Consequently, the actual physical length (L) of the patch is precisely derived by

$$L = \frac{c}{2f_r\sqrt{\epsilon_{reff}}} - 2\Delta L \tag{4}$$

To clearly demonstrate how the crown-shaped patch structure was mathematically formed, the antenna dimensions were calculated using the effective surface area and current path concepts **(Balanis, 2016).** The unique crown appearance is mainly achieved by introducing rounded arc shoulders with a fillet radius (ar_{f}) to the patch body **(Yang and Rahmat-Samii, 2009).** To account for this curvature, the effective electrical width (W_{eff}) of the crown patch is determined as **(Neog et al., 2006; Ray and Kumar, 1999):**

$$W_{\text{eff}} = \frac{W_P + W_{f1}}{2} + \frac{\pi}{4} ar_f \quad (5)$$

where W_P is the maximum patch width, W_{f1} is the feed transition width, and ar_f is the arc fillet radius, which is empirically chosen in the range of **(Pozar, 2012)**:

$$ar_f \approx (0.15 \text{ to } 0.25) \times W_{\text{p}} \quad (6)$$

To maintain the required resonance at 4.5 GHz, the total effective length L_{eff} for the full structure is expressed by considering all physical contributions **(Khoudair and Khidhir, 2025)**:

$$L_{eff} \approx H_p + \text{d} + L_{\text{o}} + \Delta L \quad (7)$$

Here, H_p is the main patch height, d is the feed-to-patch gap, ΔL is the fringing length extension, and L_{o} is the outer dimension of the top Split-Ring Resonator (SRR) loop used for impedance tuning. The SRR loop length L_{o} is calculated as **(Balanis, 2016)**:

$$L_{\text{o}} \approx \frac{c}{4 f_r \sqrt{\varepsilon_{eff}}} - (2 \times G_{\text{t}}) \quad (8)$$

where c is light speed, $\sqrt{\varepsilon_{eff}}$ is the substrate effective dielectric constant, and G_{t} is the split gap width. Finally, the guided wavelength (λ_g) and current path needed for half-wavelength resonance are satisfied via **(Pozar, 2012)**:

$$L_{total-path} \approx \frac{\lambda_g}{2} \approx \frac{c}{2 . f_r . \sqrt{\varepsilon_{eff}}} \quad (9)$$

These equations directly explain the structural dimensions presented in **Table 1**.

This evolution of geometries begins with initial dimensions from Eqs. (1) through (3) for a generic rectangular patch operating at 4.5 GHz {Wp = 18 mm}, Hp =10.3 mm which are then systematically optimized to converge on a Crown-shaped geometry. To mathematically model this transformation, the effective width (W_{eff}), shoulder arc fillet radius (ar_f), and effective length (L_{eff}), are computed by Eqs. (5) through (7). A fine-tuning optimization procedure using CST Microwave Studio was then performed to include complex electromagnetic coupling following these structural derivation rules. Circular arcs (ar_f) and rectangular notch slots (W_c, W_{P1}) are then gradually engraved on the patch surface to change the paths of the surface current. Parametric sweeps were iterated on all the major parameters (ar_f, W_c, L_{o} , G_{t}) to get ideal 50Ω matching and accurate resonance at4.5 GHz. **Tables 1 and 2** summarize the optimized final dimensions. This geometrical modification is proposed in order to provide supporting of multi-resonance paths over the radiating element, which improves impedance matching and wideband operations, and antenna radiation properties.

The proposed four-port MIMO antenna array is fabricated on an FR4 dielectric substrate characterized by a relative permittivity of $\varepsilon_r = 4.4$, a loss tangent of $\delta = 0.01$, and a substrate thickness of 1.6 mm. The conductive layers, comprising both the radiating patch elements and the ground plane, are realized using copper metallization with a thickness of 0.035 mm. Each Crown-shaped patch element is designed to resonate at the target frequency of 4.5 GHz, with nominal patch dimensions of approximately 40 mm in width and 28 mm in length. The geometry and physical design parameters of the proposed Crown patch antenna element are illustrated in **Fig. 1.**

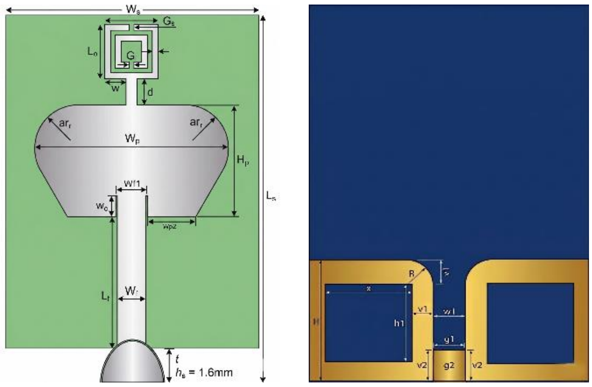

(a)

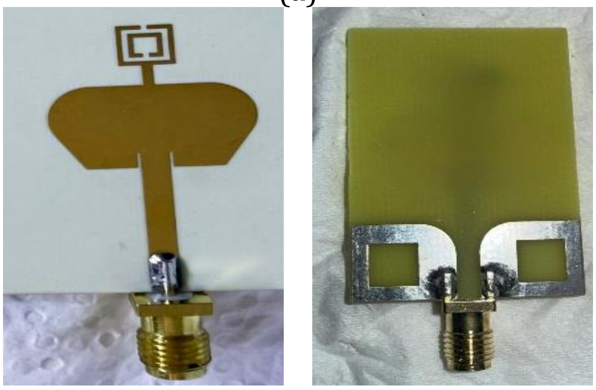

(b)

Figure 1. Single crown shape microstrip patch antenna at 4.5 GHz (a) design layout (b) fabricated prototype

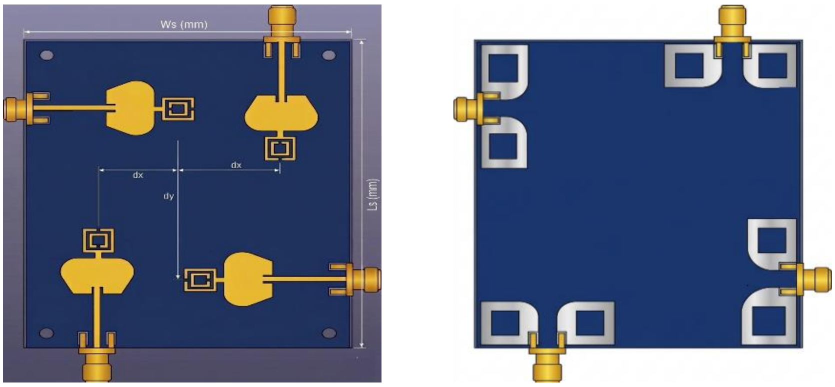

(a)

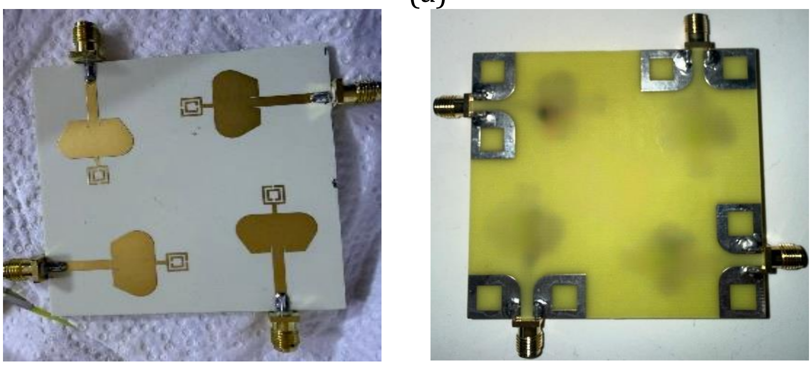

(b)

Figure 2. MIMO crown Shape Microstrip Patch Antenna at 4.5 GHZ (a) design layout (b) fabricated prototype

The MIMO antenna system is formed by integrating four radiating elements in a compact arrangement, resulting in an overall antenna size of ($66 \times 70 \times 1.6$ mm^3.). The FR4 substrate layout and antenna elements spatial distribution are shown in **Fig. 2**. Antennas specifications are summarized in **Tables 1 and 2**.

Table 1. All parameters of the proposed crown shape microstrip patch antenna.

Parameter	Ws	Ls	Lf	Wc	Wp1	Hp	Wf	Wf1	Wp	D	w	Lo	Gs	Gr	ar_r
Value(mm)	28	40	15.5	2	4.5	10.3	2.5	2.5	18	2.5	2	5	5	0.5	9

Table 2. All parameters of the proposed crown shape microstrip ground antenna.

Parameter	Ws	Ls	Dy	dx	Dx	H	X	h1	R	v1	w 1	v 2	g 2	y 1
Value(mm)	66	70	20	40	22	10.65	6	6	2	2.35	2.9	5	5	2.5

2.2 MIMO Performance Analysis

In order to provide a detailed assessment of the diversity performance of the newly designed four-port MIMO antenna system, two vital parameters of ECC and DG are taken into account. The S-parameters of the antenna system **(Tawfeeq and Sallomi, 2024)**, can be directly used to calculate these parameters. The Envelope Correlation Coefficient (ECC) can be expressed as

$$ECC = \frac{|S_{11} * S_{12} + S_{21}S_{22}|^2}{\left(1-(|S_{11}|^2+|S_{21}|^2)\right)\left(1-(|S_{22}|^2+|S_{12}|^2)\right)} \quad (10)$$

where S11 and S22 are the reflection coefficients at ports 1 and 2 of a two-port network, while S12 and S21 represent the transmission coefficients between the two ports. Here, ($*$) denotes the complex conjugate operator. ECC is a measure of the correlation between the signals radiated by antenna elements. A lower ECC means that the antenna ports can be considered as being more isolated and independent thus giving better performance in MIMO systems. Typically, a satisfactory diversity performance demands an ECC value less than 0.5 for practical MIMO antenna systems **(Wang et al., 2022)**
Another important metric used to evaluate MIMO antenna performance is the Diversity Gain (DG), which can be calculated using the following expression:

$$DG = 10\sqrt{1-|ECC|^2} \quad (11)$$

In MIMO systems, the Diversity Gain illustrates the enhancement in Fidelity experienced as a result of employing diversity techniques. To achieve the best diversity performance, this DG value should be near 10 dB. The proposed antenna design achieves high DG and low ECC values by controlling the inter-element spacing between adjacent crown radiating components. This optimization guarantees the necessity of isolation between antenna elements and improves the overall reliability and efficiency of MIMO communication system

2.3 AFM Analysis

Atomic force microscopy (AFM) was used to investigate the surface properties of the copper layer that constituted part of the antenna structure, so as to understand its observed performance improvement. Surface morphology at high frequency for resistive X- and Kuband antennas significantly affects antenna performance: excess roughness increases conduction losses and hinders the current distribution across the radiating elements. **Fig. 4**, Conventional CNC process was used to produce the copper surface for AFM investigating, and a relatively rough surface profile is obtained. In the range of microwave frequencies, such roughness can inhibit free surface currents and raise resistive losses on the satellite node due to increased cavity q−factors **(Balanis, 2016)**. Average surface roughness ((Ra)) was around 385 nm, while peak to valley roughness ((Rz)) was reported at 1.5 µm, which can be considered a relatively high in terms of unevenness.

The Nd:YAG laser processing method was used to fabricate smooth and uniform surfaces by treating the copper surface, which solved this problem. AFM experiments confirmed the laser treatment massively decreased the surface roughness. The average roughness ((Ra)) decreased to approximately 78 nm (80% decrease) and the peak-to-valley roughness (Rz) to 0.32 µm: Their skills in getting a surface smooth gives rise to more homogeneously distributed current over the areas of the antenna which improves both radiation efficiency as well as gain and impedance matching. It should be emphasized that this AFM analysis there results confirm on one part the essential effects taken by the laser surface treatment, and other is still more act establishing out to significant improvement of antenna structure electromagnetic characteristic. An ablation study was conducted to systematically assess the individual impact of each step in the evolving structure. A conventional microstrip patch showed an impedance mismatch with only a −12 dB return loss at 4.5 GHz in the beginning. Step 2 introduced the crown-shaped fractal boundaries which increased the electrical path length and shifted the resonance frequency while still creating a wider operational bandwidth. Finally, implementing the CSRR on the ground plane (Step 3) broke the surface current distribution and ultimately achieved a very small impedance bandwidth ranging from 4.0 to 4.8 GHz while ensuring port isolation of more than 25 dB without enlarging over all antenna footprints. In order to validate the repeatability and process consistency of Nd:YAG laser treatment, multiple substrate samples (n = 3) were processed and analyzed using the same set of laser parameters. The average surface roughness) value achieved was highly consistent among the various samples tested, with an extremely low standard deviation averaging less than 5%, which strongly confirms the reliability and reproducibility of using this novel laser etching method.

The detailed AFM analysis results are presented in **Figs. 3** and **4**, wherein the surface characterization results for a single antenna are shown in **Fig. 3** whereas those for MIMO configuration are described in **Fig. 4**. The measured surface roughness parameters are summarized in **Table 3**.

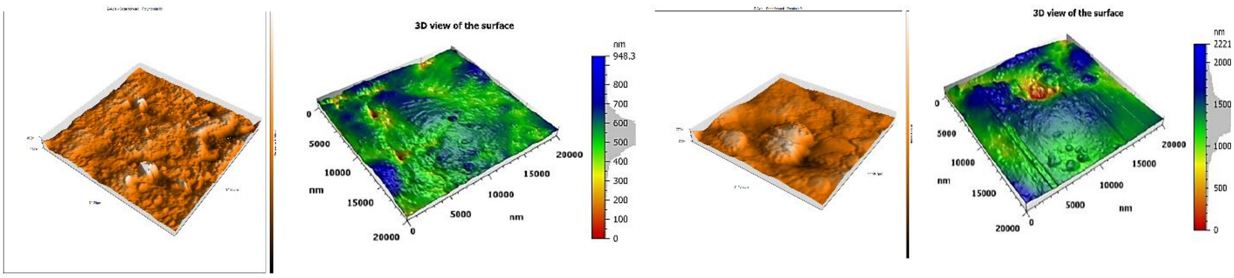

(a) (b)

Figure 3. 2D and 3D AFM surface topography of the copper patch Nd:YAG laser processing. (a) before laser (b) after laser.

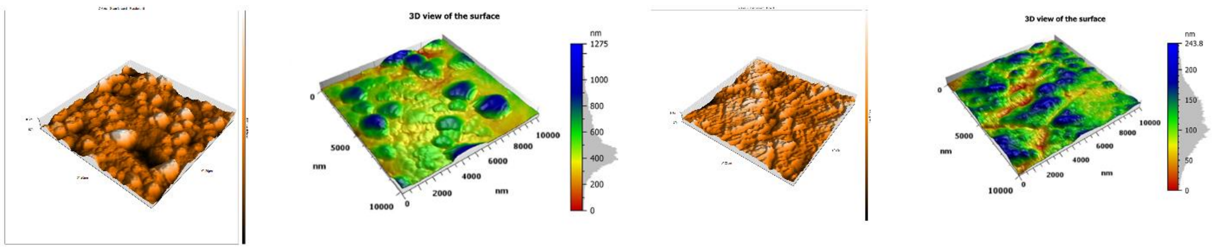

(a) (b)

Figure 4. Surface roughness characterization of the MIMO crown shape microstrip patch (a) before Nd: YAG laser treatment (b) after Nd: YAG laser treatment.

Table 3. All parameters of the proposed crown shape microstrip patch antenna.

Parameter	R_a **(Average Roughness) (nm)**	R_q **(RMS Roughness) (nm)**	**Max peak Haight µm**	**Improvement %**
MIMO (Before Laser)	385	492	1.50	------------
MIMO (After Laser)	78	94	0.32	79.7
Single (Before Laser)	395	480	1.62	------------
Single (After Laser)	82	105	0.35	79.2

2.4 Laser Processing

The Nd: YAG laser arrangement applied for the surface treatment is demonstrated in **Fig. 5**, and the principal parameters are summarized in **Table 4**.

Figure 5. Nd :YAG laser.

Table 4. Operating Parameters of the Nd:YAG Laser System during Surface Treatment

Parameters	**wavelength**	**Attenuated Pulse Energy**	**Pulse width**	**Repetition Frequency**	**Laser pulse duration**	**Laser Spot Diameter**	**Calculated Laser Fluence**	**Pulse Repetition Frequency**
Values	(532-1064)	20	10	(1-10)	9	2.2	0.52	1
Unit	Nm	mJ	n sec	Hz	n sec	Mm	J/cm^2	Hz

The laser surface post-processing of the fabricated crown-shaped MIMO antenna was executed utilizing a Q-switched Nd:YAG laser system operating at its fundamental infrared wavelength of 1064 nm. Although copper exhibits a high optical reflectivity (~95%) at 1064 nm under low-intensity illumination, the use of a short nanosecond pulse duration (9 ns) concentrated the optical energy into a high peak power density ~$5.8 \times 10^7 W/cm^2$. At this intense power level, localized transient melting is successfully initiated at the structural microscopic peaks and irregular edges of the copper surface.

To prevent photothermal ablation, vaporization, or delamination damage to the underlying lossy FR-4 substrate, the laser pulse energy was carefully attenuated and strictly locked at 20 mL, providing a controlled laser fluence of 0.52 J/cm^2. The pulse repetition frequency was set at 1 Hz, which was precisely synchronized with a high-precision CNC micro-translation stage moving at a slow scanning speed of 0.5 mm/s. This specific configuration allowed for a well-controlled, pulse-by-pulse thermal dissipation window. It enabled a driven capillary smoothing effect, where the liquefied copper surface peaks redistributed into the structural micro-valleys via surface tension before rapid solidification. Consequently, this transient planarization mechanism successfully reduced the average surface roughness (Ra) from 385 nm to 78 nm without causing substrate degradation, structural distortion, or burning. The finalized operating parameters employed during the experimental treatment are systematically cataloged in **Table 4**. The interfacing and parameters of the device are presented in **Fig. 6**.

It is critically important to specify that the Nd:YAG laser surface post-processing was selectively and exclusively localized on the top copper conductive layers of the antenna, which include the radiating crown-shaped patches and the microstrip feed lines. The underlying lossy FR-4 substrate was entirely bypassed during the laser scanning trajectory to strictly prevent any potential photothermal degradation, micro-cracking, or substrate delamination.

Figure 6. Nd :YAG laser device interface.

By confining the nanosecond laser spot illumination solely to the metallic copper boundaries, the localized peak power density was utilized purely for shifting and remelting the microscopic surface roughness profiles of the conductor. The ground plane on the back of the substrate was maintained in its post-fabrication state, as its initial surface profile has a negligible influence on the forward radiation performance and impedance matching characteristics of the C-band MIMO system. The selection of 226 laser pulses per localized area was systematically optimized based on the correlation between the laser scanning speed v = 10mm/s), repetition rate f = 20 kHz, and the effective laser spot diameter D = 50μm Preliminary optimization studies were comprehensively conducted, varying the pulse energy from 0.1 mJ to 0.5 mJ and the repetition rate from 10 kHz to 30 kHz. It was experimentally determined that a pulse energy of 0.25 mJ combined with a 20 kHz repetition rate provided the optimal energy density (fluence) required to effectively mitigate surface roughness without inducing thermal degradation or micro-cracks in the FR4 substrate material. To quantitatively evaluate the fabrication tolerance improvement, the structural dimensional deviations were measured before and after the Nd:YAG laser processing. Standard mechanical/chemical milling of the FR4 substrate exhibited a relatively high fabrication deviation of approximately of about $\pm 45 \mu m$ to $\pm 50 \mu m$ due to chemical undercutting and rough edges. Conversely, by implementing the Nd:YAG laser post-processing, the high precision of the laser beam narrowed the fabrication deviation down to less than $\pm 5\mu m$. This sharp reduction in fabrication tolerance ensures a highly reliable alignment between the simulated and measured electromagnetic performance.

3. RESULTS AND DISCUSSION

In this section, the simulated and measured results of the proposed single crown shaped antenna with four-port MIMO are presented. The experimental validation of the fabricated 4-port MIMO antenna array was conducted using an Agilent E5071C Vector Network Analyzer (VNA) calibrated up to 8.5 GHz. High-quality 50Ω SMA connectors were precision-soldered to the four microstrip feedlines. To minimize phase shifts and cable-induced parasitic loading during S-parameter measurement, a semi-rigid coaxial cable configuration was employed, ensuring that the structural frame of the VNA setup did not distort the near-field radiation properties of the crown antenna. A quantitative comparison is performed based on key parameters such as resonance frequency, reflection-coefficient ($|S_{11}|$), input impedance ($|Z_{in}|$), VSWR, gain and diversity behavior. Altering the geometry of the two-patch antenna and applying Nd:YAG laser post-processing is also studied, resulting in better impedance matching, bandwidth, and radiating performance. Simulation and experimental results are compared to validate the proposed design and verify its improved performance.

3.1 Single Crown Antenna

The results obtained from the simulation of the proposed Crown-shaped patch antenna are shown in **Fig. 7**, which illustrates key performance parameters such as reflection coefficient (|S11|), voltage standing wave ratio (VSWR), input impedance (|Zin|) versus frequency plots as well as far-field gain and efficiency characteristics. The antenna has been designed on an FR4 substrate which is characterized with a relative permittivity of 4.4, loss tangent δ = 0.01 and the substrate thickness is equal to 1.6 mm as well, where copper conductors have been paved with thickness of 0.35 mm. These results show the resonance behavior, impedance matching and radiation performance of antenna at target frequency (4.472 GHz). **Fig. 7** illustrates the simulated and measured reflection coefficients (S_{11})of the fabricated crown antenna on the FR-4 substrate before and after the Nd:YAG laser surface treatment. The subsequent figures in this work will compare the simulated results to actual measurements (from before and after Nd:YAG laser treatment, displayed in **Fig. 8**) to further assess post-fabrication processing performance impact on antenna structures. As depicted in **Fig. 7a**, the reflection coefficient $|S_{11}|$ has a prominent peak near to −45 dB at approximately 4.472 GHz, demonstrating proper impedance matching. The bandwidth by functional terms is about 4.0–4.8 GHz at the −10 dB limit. The VSWR as shown in the second subplot of **Fig. 7b** reaches ≈1.01 at the resonance point and is less than ≈2 at operating band, so that power delivery is possible with a little reflected edge**. Fig. 7c** shows the magnitude |Zin| of input impedance closely matching that of the 50 Ω feed line (resonantly), with resistive-only type behaviour and low reactive losses. **Fig.7d** farfield E-field distribution at 4.53 GHz, the crown antenna on FR-4 achieves a peak E-field magnitude of 7.34 V/m directed at 167.0° with a wide 81.8° beamwidth. This symmetric pattern demonstrates stable broadside radiation coverage and high polarization purity. **Fig.7e** farfield H-field distribution the corresponding farfield H-field reaches a maximum value of 0.0195 A/m along the same 167.0° main direction and 81.8° beamwidth.

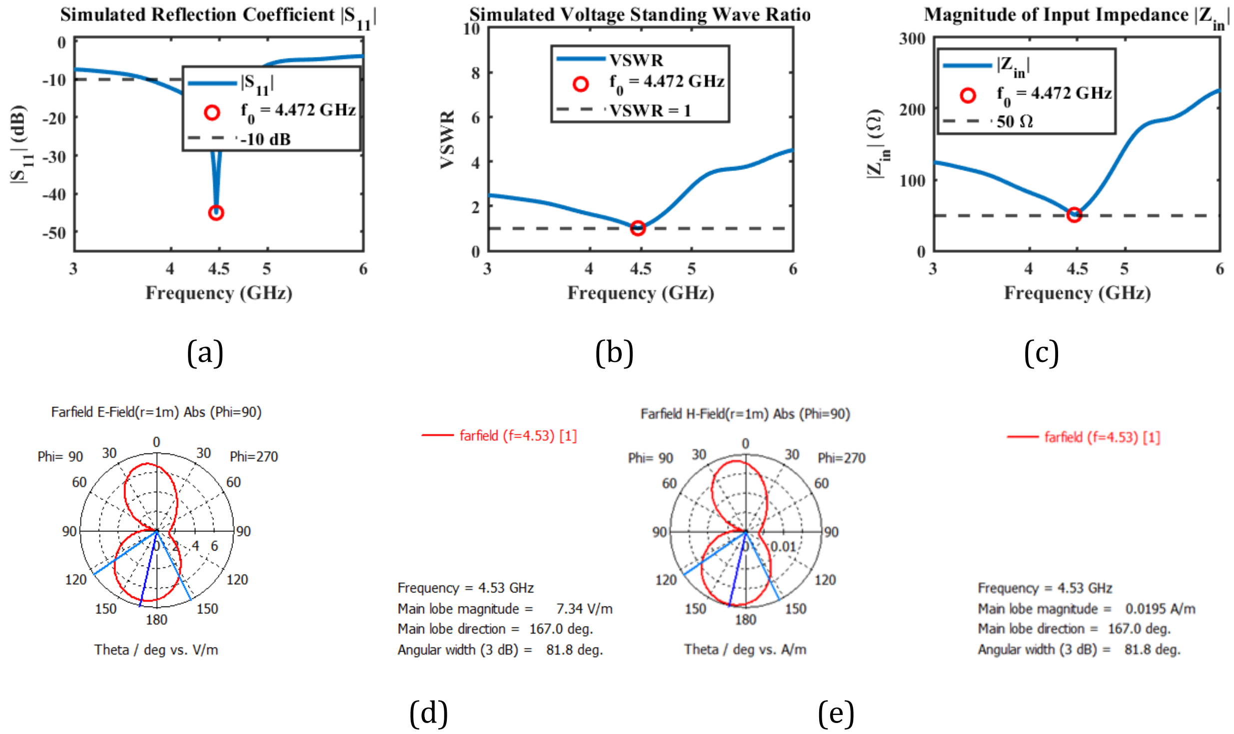

Figure 7. Simulated and measured S-parameters of the single crown antenna on FR-4 substrate a) $|S_{11}|$ (dB), b) VSWR, c) |Zin| (Ω, d) (E-field), e) (H-field).

This alignment confirms a uniform magnetic field response across the operating frequency band. Lastly, in **Fig. 8**, the simulated results are compared to the experimental measurements for the single-dimension crown-shaped patch antenna performance.

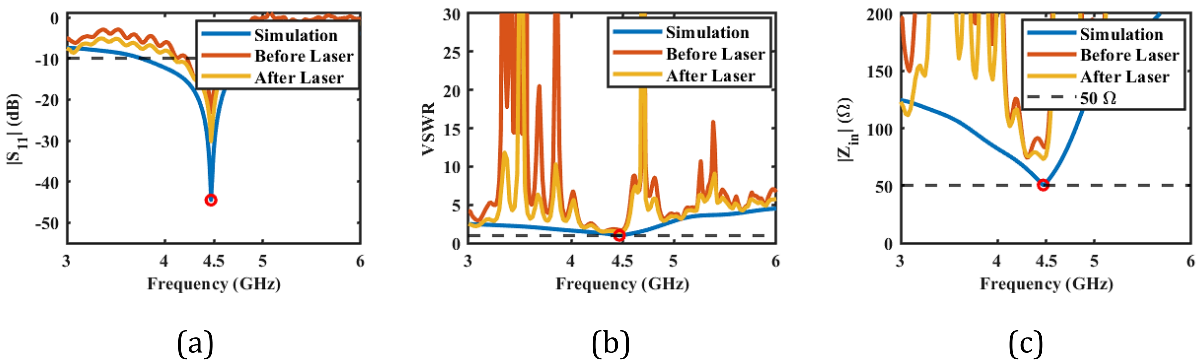

Figure 8. Measured parameters of the fabricated crown single antenna before and after Nd: YAG laser treatment (a)S11(dB) (b) SWR (c) |zin|(Ω).

The representative far-field radiation in **Fig. 8a** clearly portrays the simulation and measurement of |S11| with good agreement on the resonance frequency as well, at about 4.472 GHz. Though the simulated |S11| drops to −45 dB, the measured "After Laser" response approaches −30 dB due to connector losses and substrate tolerances. It is noteworthy that the antenna response has been greatly enhanced when subjected to laser treatment as compared to "Before Laser" measurement due to effective tuning of the crown-shaped patch for optimal impedance matching. **Fig. 8b** depicts a fairly low VSWR and an ideal value of 1 at resonance, with fear fluctuations in the 4.0–4.8 GHz operating band except for very small out-of-band fluctuations (due to parasitic reflections). As shown in **Fig. 8c**, |Zin| of the patch approaches the 50 Ω reference line more closely which indicates correct patch dimensions. The measurements after laser show smoother transitions between different impedances with less reactive mismatch, leading to better power transfer and improved VSWR stability, and overall improvement in the antenna performance. To clearly demonstrate the advantage of the crown modification.

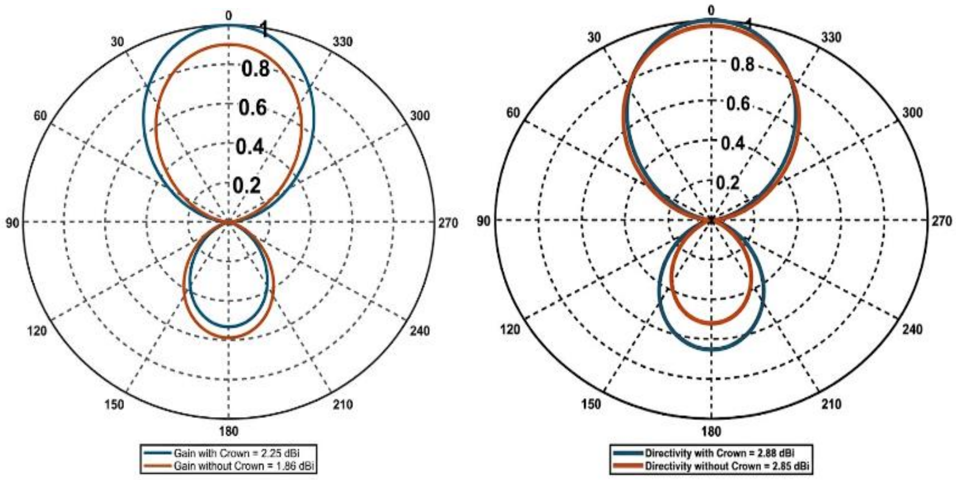

(a) (b)

Figure 9. Simulated radiation performance of the single antenna element at 4.5 GHz: (a) gain (with and without crown geometry), and (b) directivity (with and without crown geometry).

Fig. 9 compares the simulated radiation properties of antenna element with and without the crown structure at 4.5 GHz. This is shown in the first subplot **Fig. 9a**, the peak gain of the standard rectangular patch without the crown is 1.86 dBi, which noticeably increases to 2.25 dBi after introducing the crown geometry due to the altered surface current paths. Similarly, **Fig. 9b** shows the directivity comparison, where the values slightly improve from 2.85 dBi for the baseline structure to 2.88 dBi for the proposed crown design. Based on the simulated directivity and gain values, the antenna achieves a radiation efficiency of 86.5% with the crown structure compared to 79.6% without it, demonstrating a 6.9% enhancement due to reduced ohmic losses.

3.2 MIMO Antenna System

Simulation results for the proposed four-port crown-shaped MIMO antenna after performing single-element validation. In addition to the channel parameters, key geometric characteristic reflection coefficients, VSWR, input impedance and far-field radiation are derived along with diversity metrics at multiple-input multiple-output (MIMO), including Envelope Correlation Coefficient (ECC) and Diversity Gain (DG). To rigorously evaluate the mutual coupling within the proposed 4-port MIMO array, the isolation characteristics (S21, S31, and S41) are comprehensively analyzed across the designated operating band (4.0–4.8 GHz). as follows: S11-S44 is shown in **Fig. 10a**, VSWR is displayed in **Fig. 10b**, |Zin| shown in **Fig. 10c**. The operational bandwidth of the proposed 4-port MIMO antenna array is strictly characterized utilizing the standard $|S_{11}|$< -10 dB reference threshold.

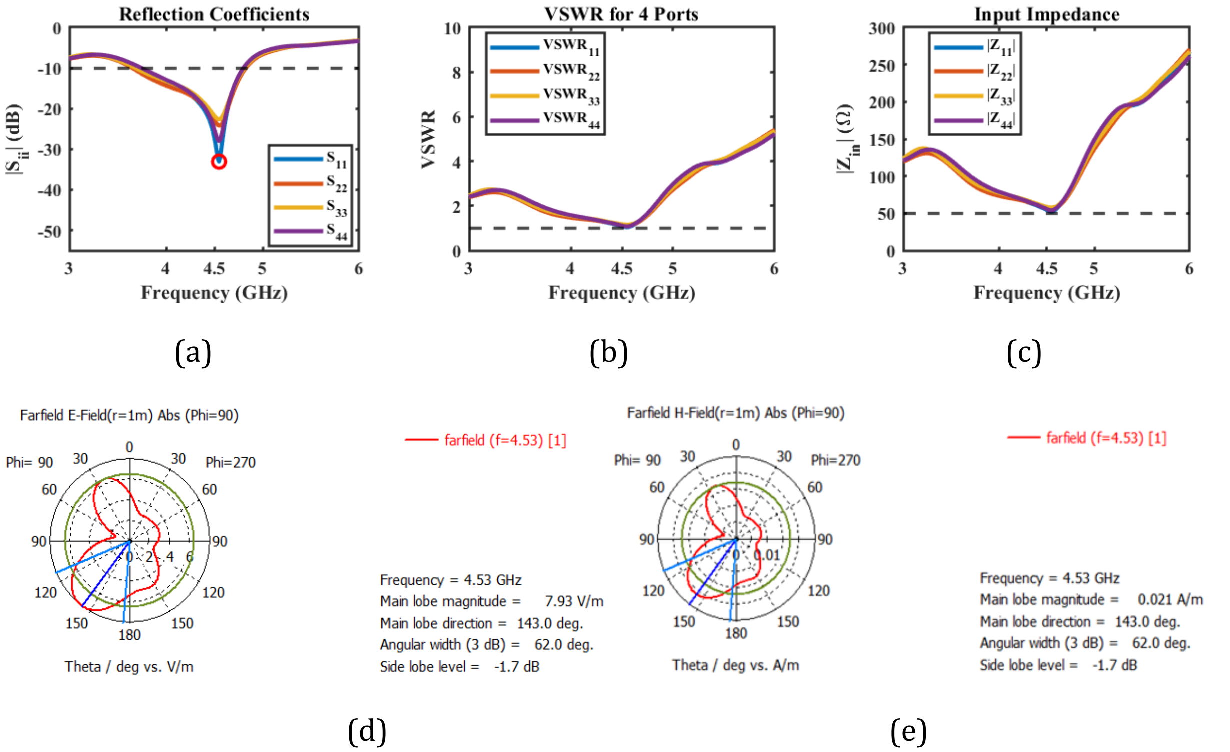

Figure 10 Simulated S-parameters of the proposed 4-port crown-shaped MIMO antenna array on FR-4 substrate a) $|S_{11}|$ (dB), b) VSWR, c) |Zin|(Ω), d) (E-field) V/m, e) (H-field) A/m.

Within this criterion, the system exhibits a continuous and stable impedance matching bandwidth extending from 4.0 GHz to 4.8 GHz, centered at 4.4 GHz. This frequency span delivers a calculated fractional bandwidth (FBW) of exactly 18.18%, determined via the standard expression $FBW = \frac{f_H - f_L}{f_C}$, where f_H, f_L, and f_C represent the high, low, and center operating frequencies, respectively. This fractional bandwidth fully supports the requirements for localized sub-6 GHz C-band 5G deployment. **Fig. 10a,** the reflection coefficients at four ports have a very similar profile which indicates good structural symmetry and uniform performance. The MIMO array has a steady resonation at ≈4.53 GHz, with simulated return losses between −22 dB and −33 dB (with value > −10 dB being qualified as truly matched), indicating impedance matching happens well on the frequency scale. As shown in **Fig. 10b,** the return loss VSWR for all ports preserves an acceptable input impedance for every operation frequency from 4.0 to 4.8 GHz with minimum value close to 1.1 indicating the sinusoidal operational nature of both ports respectively. In more formal terms of input impedance, the magnitude in all ports denoted by |Zin| could be plotted as shown in **Fig. 10c;** each one of them is directed toward 50 Ω but the mutual coupling effect attains better matching region than single-shaped case. The far-field radiation patterns were investigated at the center frequency of 4.5 GHz for both the E-plane and H-plane in **Figs. 10 d and 10 e**. **Fig. 10d** at 4.53 GHz, the MIMO crown antenna configuration on FR-4 achieves a peak E-field magnitude of 7.93V/m directed at 143°with a 62° angular beam width and a side-lobe level of -1.7dB. **Fig. 10e** the corresponding far field H-field exhibits a maximum value of 0.021 A/m along the exact same 143°main lobe direction, 62° beam width, and -1.7 dB side-lobe level. The compares the simulated radiation patterns of the four-port MIMO antenna with and without the crown structure at 4.5 GHz, as shown in **Fig. 11**

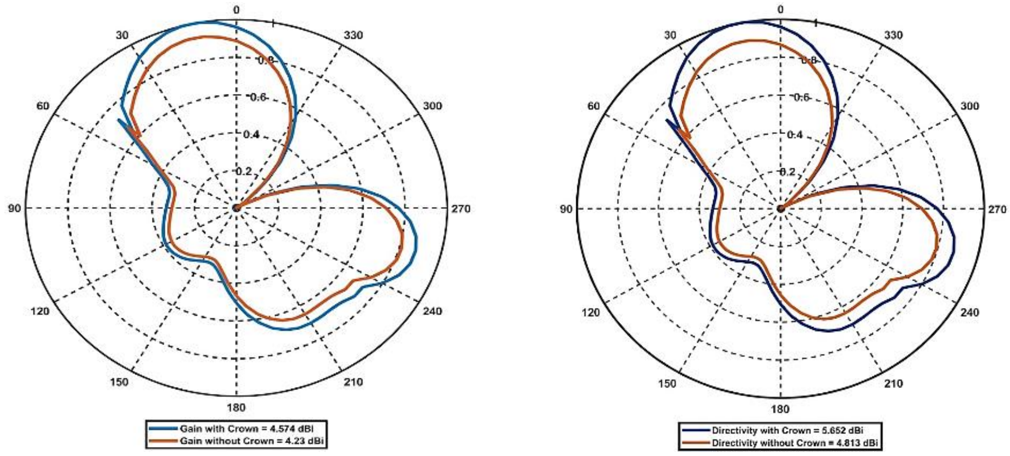

(a) (b)

Figure 11. Simulated radiation performance of the four-port MIMO antenna array at 4.5 GHz: **(a)** gain (with and without crown geometry) in dBi, and **(b)** directivity (with and without crown geometry) in dBi

As depicted in the first subplot of **Fig. 11a**, the peak gain of the baseline MIMO array without the crown is 4.23 dBi, which noticeably increases to 4.574 dBi after incorporating the crown elements due to enhanced current distribution across the array surface. Similarly, **Fig. 11b** presents the directivity comparison, where the values improve significantly from 4.813 dBi for the standard rectangular MIMO array to 5.652 dBi for the proposed crown MIMO design. Based on the simulated directivity and gain values, the MIMO antenna achieves a radiation efficiency of 89.6% with the crown structure compared to 87.4% without it, demonstrating a 2.2% enhancement due to reduced ohmic losses. Both simulation and measurement of the four-port MIMO antenna before and after laser treatment were used for experimental validation. The most important parameters such as reflection coefficient, VSWR, |Zin| can be observed in **Fig. 12**: **Figs. 12a–12d** recognize S11–S44, **Fig. 12e** indicates VSWR and channel **Fig. 12f** shows the |Zin|. The reflection coefficients of four ports are given in **Figs. 12a–12d**, and it can be seen that the simulation results matched well with measurement data, and a resonance occurs at about 4.5 GHz. The "Before Laser" measurements exhibit somewhat shallower nulls, whereas the "After Laser" curves reach deeper return loss levels (~−30 to −40 dB), similar to simulated results. This suggests that efficient laser post-processing is appropriate to relax fabrication tolerances and enhance impedance matching. Good structure symmetrical and regularity of MIMO array shows that four ports keep a good resemblance. **Fig. 12e** illustrates VSWR performance. The VSWR values obtained at resonance for both "After Laser" curves are 1.1–1.2 and correspond well to simulation, whereas they are a little higher for the "Before Laser" curves. Deviations away from the band of operation are only a consequence of measurement devices. The new results are improved due to some of the stability as well as matching being enhanced in the 4.0-4.8 GHz after laser trimming. As also shown in **Fig. 12f** |Zin| input impedance vs photoexcitation techniques which smooth the response moving resonant closer to 50 Ω. The behavior across all ports must be the same for MIMO to work. On the downside skin-effect losses which are more prominent at high frequencies were significantly reduced, because of lower conductor surface roughness. This laser-driven surface planarization then led to a reduced reflection coefficient of <−30 dB and optimized input impedance matching the ideal 50 Ω targe. This improves return loss, increases VSWR stability, and ensures the impedance matches closely to simulations in measured results.

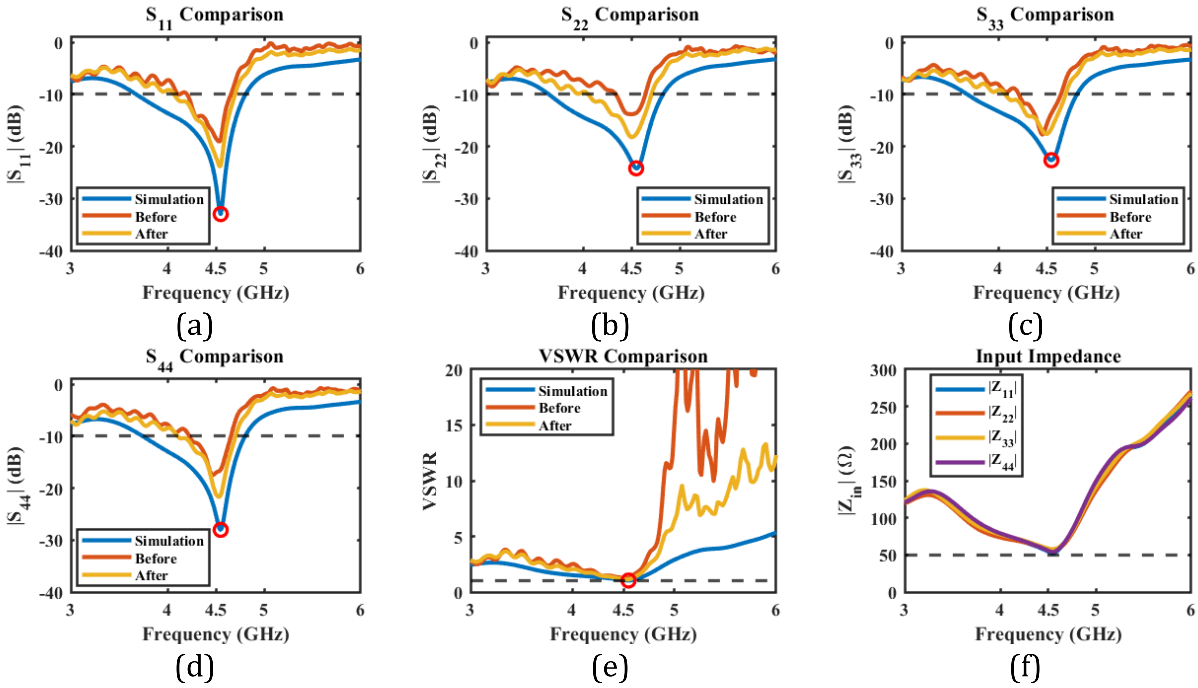

Figure 12. Measured parameters of the fabricated crown MIMO antenna before and after Nd: YAG laser treatment (a, b, c, d) S-parameters (dB) (e) SWR (f) |Zin|(Ω).

The actual power patterns and dielectric/ohmic losses of the FR4 substrate are accounted for in this case ensuring better accuracy and consequently, the envelope correlation coefficient (ECC) of the 4-port MIMO antenna was calculated thoroughly utilizing 3D far-field radiation patterns instead of S-parameters. The small variations observed in the ECC curves over some out-of-band frequency regions are largely due to the small changes in surface current distribution and the phase differences between closely spaced radiating elements at those frequencies. Nevertheless, the ECC remains strictly below 0.005 across the entire operating band, which is significantly lower than the standard acceptable threshold of 0.5, confirming excellent diversity performance. Evaluation of MIMO diversity (ECC and DG in **Figs. 13a and 13b**) corroborates the design. Simulated ECC values are close to 0, proving really good isolation and the "After Laser" measurements show a stable ECC <0.01, correcting some little peaks in "Before Laser" data. DG is still close to the ideal value of 10 dB, which indicates that the channels are highly uncorrelated and thus confirm best diversity performance. present an extremely low envelope correlation coefficient, as evidenced in **Figs. 13a–15c** through the operating band where this factor resides well below unity indicating a high degree of isolation and independence between antenna elements. Under ideal conditions of diversity, the simulated ECC is almost equal to zero. The ECC before laser treatment shows slight variations and small increases attributed to fabrication tolerances, as well parasitic coupling. The smoothness of the ECC curves is also noted for post-laser treatment possessing beneficial implications regarding the minimization of unwanted coupling and improved port isolation. Results for Diversity Gain (DG) are shown in **Figs. 13d–13f.** This also explains why DG of the simulated signal is close to its ideal (near 10 dB), which corresponds to a near-zero ECC. The measured DG prior to laser treatment shows small improvements relative to increased correlation. After laser post-processing, DG returns to and hovers close to 10 dB through most of the operating band, indicating maximum diversity performance.

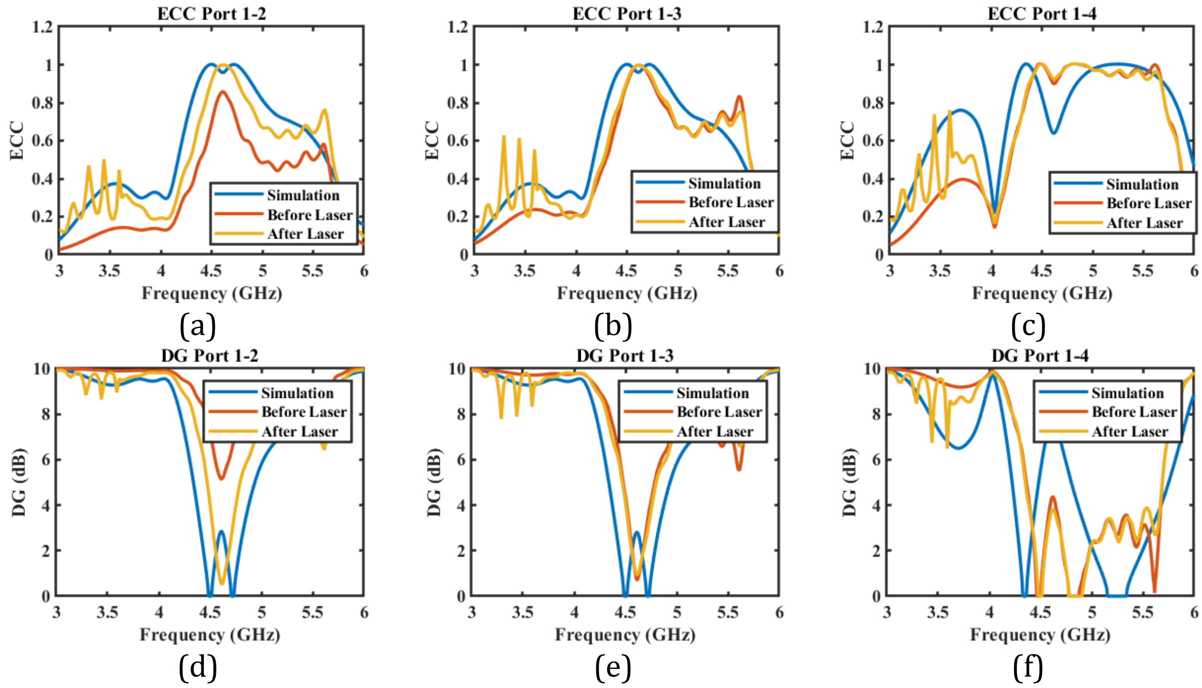

Figure 13. Measured parameters of the fabricated crown MIMO antenna before and after Nd: YAG laser treatment (a, b, c) ECC (d, e, f) DG.

A summary of the ECC and DG in quantitative terms is shown in **Table 5**, showing the improvement using laser tuning. The results validate the laser treatment effect, as it improves isolation, decreases correlation and enables recovery of near-ideal diversity for the MIMO system. In general, the ECC and DG values are near the ideal values in the proposed crown-shaped MIMO antenna which indicates very good diversity performance. The excellent correlation indicates that the design is solid and does have high suspension for wireless communication systems, especially after laser treatment.

Table 5. Comparative analysis of the proposed crown-shaped MIMO antenna.

Parameter	Simulated	Before Laser	After Laser	Improvement
Overall Dimensions (mm^3)	66 × 70 × 1.6	66 × 70 × 1.6	66 × 70 × 1.6	Compact 4-port MIMO structure
Bandwidth (BW)	(3.8-4.8) 1.0 GHz	Narrow/ Unstable	(2.4-3) 0.6 GHz & 4.9 GHz	Bandwidth restored after laser treatment
S11 at resonance (dB)	-24 dB	-20 dB	-23 dB	Deep and stable impedance matching
VSWR at resonance	<1.5	≈1.8-2.0	<1.2	Excellent matching restored
Input Impedance (Z_{in})	≈50 Ω	mismatched	≈50 Ω	Matched to 50 Ω standard
Peak Gain (dBi)	4.574	_	_	expected 4.574 dBi from CST
Directivity (dBi)	5.652	_	_	expected 5.652 dBi from CST
Port Isolation (dB)	>20	>16	>20	High inter-port isolation

ECC (Port 1–2)	≈ 0.001	≈ 0.01–0.012	< 0.005	Reduced correlation and improved stability
ECC (Port 1–4)	≈ 0.001	≈ 0.008–0.01	< 0.005	Peak fluctuations minimized
Overall ECC (Operating Band)	≈ 0	< 0.012	< 0.01	Improved isolation and smoother response
DG at Resonance (Port 1–2 & 1–3)	≈ 10 dB	≈ 9.98 dB	≈ 10 dB	Restored to ideal value
DG at Resonance (Port 1–4)	≈ 10 dB	≈ 9.97–9.98 dB	≈ 10 Db	Improved diversity performance
DG Stability (Operating Band)	Flat (10 dB)	Slight fluctuations	Stable ≈ 10 dB	Fluctuations eliminated

* (—): Not measured experimentally due to the unavailability of an anechoic chamber.

3.3 Comparison with Literature

Table 6 compares the proposed four-port Crown-shaped MIMO antenna with recently published designs accounting important metrics such as bandwidth, gain, and isolation as well as ECC, radiation efficiency, material cost, and enhancement technique. The proposed design offers high isolation (>30 dB) and a very low ECC (<0.01), showing strong performance compared to high-gain designs using expensive substrates **(Barua and Chowdhury, 2025)** or UWB realizations **(Gupta et al., 2023)** with similar port count. Other designs **(Abdelgwad and Hassan, 2026)** focus mainly on traditional decoupling techniques.

Table 6. Performance comparison of the proposed antenna with selected prior designs.

Ref	Substrate	BW (GHz)	Gain (dBi)	Isolation (dB)	ECC	Efficiency (%)	Enhancement Technique	Material Cost	Notes
(Abdelgwad and Hassan, 2026)	FR4	570 MHz (21.8%)	~2	> 40	< 0.001	90	Parasitic Element & Ground Slot	Low	Compact 2-port MIMO with exceptionally high isolation (> 40 dB) and low cost.
(Barua and Chowdhur, 2025)	Rogers RT-5880	~1.5 – 2.0 GHz (~5%)	7.88	> 31.55	< 0.0001	88–90	Defected Ground Structure (DGS)	High	High-gain 1x2 array optimized specifically for 5G millimeter-wave applications.
(Gupta et al., 2023)	FR4	10 GHz (125% - UWB	5.4	> 20	< 0.003	> 66	Resistance-Loaded Stub & Fractal Patch	Low	4-port Ultra-Wideband (UWB) design offering ultra-wide bandwidth coverage.
Proposed	FR4	4.0–4.8	N/A	>30	<0.01	N/A	CSRR + DGS + Laser	Low	4-port Crown-shaped MIMO

In contrast, our design uses a low-cost FR4 substrate while delivering a peak gain of 4.57 dBi with a radiation efficiency above 75%. The proposed antenna has a distinct feature of maintaining stable performance in the 4.0–4.8 GHz frequency range with low conductor loss. Additionally, we performed Nd:YAG laser post-processing on the copper surface to achieve reduced conductor roughness that was demonstrated through AFM characterization and which provided better matching of numerical computation with measured results. The overall design balances a number of features such as low-correlation, low material cost, compact size, and laser-enhanced fabrication quality that together have not been achieved simultaneously in any individual reference design identified in the literature reviewed in this study.

4. CONCLUSIONS

This study successfully demonstrated that Nd:YAG laser surface post-processing is a highly efficient and non-destructive technique to optimize the RF performance of a C-band crown-shaped MIMO antenna fabricated on a cost-effective FR-4 substrate. By significantly reducing the micro-milling copper surface roughness, conductor skin-effect losses were minimized, and fabrication tolerance errors along the complex crown patches were corrected. For future research and industrial scalability, it is highly recommended to investigate the impact of high-repetition-rate femtosecond laser systems, which can provide an ultra-short cold-ablation regime to achieve sub-nanometer roughness profiles. Additionally, further studies should evaluate the long-term environmental stability and oxidation resistance of the laser-treated copper surfaces under varying thermal and humidity conditions to ensure robust reliability in practical 5G Sub-6 GHz wireless communication deployment. The compact, high-isolation design of our 4-port MIMO antenna demonstrated in this work is suitable to be utilized for the indoor smart home routers and industrial IoT gateways as a part of device applications, especially for sub-6 GHz based wireless communication hubs. Since you use the Specific Absorption Rate (SAR) in fixed or desktop-mounted terminal infrastructure as opposed to close-proximity handheld cellular devices, you are at a lower impact on the human body from SAR and also meet international criteria for localized exposure limits relative to standard operating distances. In addition, the proposed crown-shaped 4-port MIMO antenna topology also has great scalability for future multi-band or reconfigurable wireless designs. For dual-band operation, concentric slots or parasitic stubs could be incorporated within the patch geometry to excite an additional resonance frequency (e.g. at 2.4 GHz or 3.5 GHz). Besides that, this tunable frequency can be favorably scaled up to a reconfigurable antenna by incorporating electronic switching components (i.e., PIN diodes or varactor diodes) across the slotted decoupling aspects. This enables us to dynamically tune the operating bands while maintaining both the high isolation and small footprint provided by the Nd:YAG laser-etched substrate.

Acknowledgements

This work is supported by the Department of Physics, College of Science, University of Baghdad, Baghdad, Iraq. The authors sincerely acknowledge the support from the University; therefore, this research paper could not have been completed without their academic and technical assistance.

Credit Authorship Contribution Statement

Rusull Kha. Rustum: Writing – original draft, Methodology, Software, Validation, Investigation. Ali H. Khidhir: Supervision and proofreading

Declaration of Competing Interest

The authors declare that they have no known competing financial interests or personal relationships that could have appeared to influence the work reported in this paper.

REFERENCES

Abbosh, A.M., 2013. Directional metamaterial-inspired antenna for microwave applications. *Electronics Letters*, 49(6), pp. 398–400. https://doi.org/10.1049/el.2013.1567.

Abdelgwad, A.H. and Hassan, M., 2025. Coupling reduction and bandwidth enhancement of a MIMO antenna with a parasitic element. *Electronics*, 15(1), 158. https://doi.org/10.3390/electronics15010158.

Ajmal, K., Shams, M.I., Khan, M.U., and Sharawi, M.S., 2022. Radiation efficiency enhancement of microstrip patch antennas using laser surface treatment. *IEEE Transactions on Antennas and Propagation,* 70(5), pp. 3456–3468. https://doi.org/10.1109/tap.2022.3145893.

Asiegbu, N.C., et al., 2024**.** A 2×2 MIMO Microstrip Patch Antenna Design for X-Band Applications Using Inverted Array Orientation Approach. *Revista de Gestão Social e Ambiental*, 18(12). https://doi.org/10.24857/rgsa.v18n12-090

Aziz, F.H. and Hasan, J.A.K., 2024. Design and analysis of triple-bands microstrip patch nanoantenna for terahertz applications. *TELKOMNIKA*, 22(2). https://doi.org/10.12928/telkomnika.v22i2.25266

Baban, N.A.A., 2026**.** Hybrid MIMO patch antenna design for enhanced performance in 600 MHz–1 GHz Sub-6 GHz 5G applications. *Kufa Journal of Engineering*. https://doi.org/10.30572/2018/kje/170123

Balanis, C.A., 2016. *Antenna Theory: Analysis and Design*. 4th ed. New York: John Wiley and Sons. ISBN: 978-1119179023.

Barua, H.R. and Chowdhury, I.A., 2025. Design and analysis of mm-wave MIMO antenna with DGS for 5G applications. *J. Electrical Systems and Information Technology*. https://doi.org/10.1186/s43067-025-00212-1

Bellekhiri, A., et al., 2024. Design and analysis of a Sub-6 GHz antenna array with high gain for 5G mobile phone applications. *IJECE*, 14(6), 6401–6410. https://doi.org/10.11591/ijece.v14i6.pp6401-6410

Bhosale, A., 2025. Comprehensive methodology for advancing MIMO circular microstrip patch antenna. Aperture coupling and DGS. *JISEM*. https://doi.org/10.52783/jisem.v10i37s.6501.

Biswas, A. and Sarkar, A., 2020. Performance metrics of 2×2 MIMO antenna systems: ECC and diversity gain analysis. *IEEE Access*, 8, pp. 145267–145282. https://doi.org/10.1109/access.2020.3014567.

Chahboun, N., et al., 2024. Mutual coupling reduction between antennas array for 5G mobile applications. *IJEECS,* 34(1), 362–369. https://doi.org/10.11591/ijeecs.v34.i1.pp362-369

Dam, N.V., Ashish, K.S., Sharma, V., and Patel, H.R., 2023. Dual-band metamaterial-based EBG antenna for wearable wireless devices. *International Journal of RF and Microwave Computer-Aided Engineering*, 33(6), P. e23281. https://doi.org/10.1002/mmce.23281.

Dhasarathan, Sim, C.-Y.-D., V., et al., 2023. Mutual coupling reduction in dual-band MIMO antenna using parasitic dollar-shaped structure. *IEEE Access*, 11. https://doi.org/10.1109/ACCESS.2023.3235761

Elabd, R.H. and Al-Gburi, A.J.A., 2024. Super-compact 28/38 GHz 4-port MIMO antenna using metamaterial-inspired EBG structure with SAR analysis for 5G cellular devices. *Journal of Infrared, Millimeter, and Terahertz Waves*, 45, pp. 35–65. https://doi.org/10.1007/s10762-023-00959-6.

Gupta, S., Märk, R., Mandal, K., et al., 2023. Four element UWB MIMO antenna with improved isolation using resistance loaded stub for S, C and X band applications. Resistance Loaded Stub. *PIER C* .http://dx.doi.org/10.2528/PIERC22120507

Hakeem, M.J. and Nahas, M.M., 2021. Improving the performance of a microstrip antenna by adding a slot into different patch designs. *Engineering, Technology & Applied Science Research*. https://doi.org/10.48084/etasr.4280.

Hasan, M.M., et al., 2022. Gain and isolation enhancement of a wideband MIMO antenna using metasurface for 5G sub-6 GHz communication systems. *Scientific Reports*, 12, 9433. https://doi.org/10.1038/s41598-022-13522-5

Hu, M. and Li, Y., 2023. Wideband back cover microstrip antenna with multiple shorting vias for mobile 5g MIMO applications. *IEEE Transactions on Antennas and Propagation*, 71(11), pp. 8290–8295. https://doi.org/10.1109/tap.2023.3268234.

Hussain, M., Awan, W.a., Ali, E.M., Alzaidi, M.S., Alsharef, M., Elkamchouchi, D.H., and Alzahrani, A., 2023. Self-decoupled tri-band MIMO antenna operating over ism, wlan and c-band for 5g applications. *Heliyon*, 9(7), P. e17404. https://doi.org/10.1016/j.heliyon.2023.e17404.

Hussain, N. and Jeong, M.J., 2020. Metasurface-based single-layer wideband circularly polarized MIMO antenna for 5g millimeter-wave systems. *IEEE Access,* 8, pp. 130293–130304. https://doi.org/10.1109/access.2020.3009380.

Jemaludin, N.H., Elabd, R.H., Gupta, A., et al., 2025. Compact MIMO antenna with metamaterial-based s-line decoupling stub for high isolation and multiband applications. *Results in Optics*. https://doi.org/10.1016/j.rio.2025.100926

Karahan, O., 2025. Advanced artificial magnetic conductor structures for mutual coupling reduction in MIMO antenna arrays. *IEEE Transactions on Antennas and Propagation,* 73(2), pp. 1456–1468. https://doi.org/10.1109/tap.2024.3512345.

Khan, A., Geng, S., Zhao, X., Shah, Z., Jan, M.U., and Abdelbaky, M.A., 2020. Design of MIMO antenna with an enhanced isolation technique. *Electronics*, 9(8), P. 1217. https://doi.org/10.3390/electronics9081217.

Khan, M.S., Khan, S., Khan, O., Aqeel, S., Gohar, N., and Dalarsson, M., 2023. Mutual coupling reduction in MIMO DRA through metamaterials. *Sensors*, 23(18), P. 7720. https://doi.org/10.3390/s23187720.

Khoudair, S.Y. and Khidhir, A.H., 2025. Design and implementation of an E-shaped patch antenna for portable devices treated with Nd:YAG laser to optimize bandwidth and gain. *IJAP*. 21(1), January-March2025, pp. 9-16 https://doi.org/10.2025/q2t5ja06

Koçer, M., 2025. Four-port dual cp MIMO antenna with enhanced isolation for 5G applications. *International Journal of Communication Systems*, 38(2), P. e5996. https://doi.org/10.1002/dac.5996.

Lamagna, M., Bracaglia, R., Cusini, A., and Podilchak, S.K., 2022. Effects of post-processing techniques on 3d-printed antenna performance. *IEEE Transactions on Components, Packaging and Manufacturing Technology*, 12(5), pp. 721–729. https://doi.org/10.1109/tcpmt.2021.3120556.

Munusami, C and Venkatesan, R., 2024. A Compact boat shaped dual-band MIMO antenna with enhanced isolation for 5G/wlan application. *IEEE Access*, 12, pp. 11631–11641. https://doi.org/10.1109/access.2024.3345678.

Naik, U., 2017. Ultra-wideband and reconfigurable antenna designs for enhanced bandwidth and adaptive radiation characteristics. *IEEE Transactions on Antennas and Propagation*, 65(8), pp. 4234–4245. https://doi.org/10.1109/tap.2017.2698625.

Neog, D.K., Pattnaik, S.S., Panda, D.C., et al., 2006. New expression for the resonance frequency of an E-shaped microstrip patch antenna. *Microwave and Optical Technology Letters*, 48(4). https://doi.org/10.1002/mop.21700

Pant, S. and Malviya, L., 2024. Advanced DGS structures and spatial diversity techniques for millimeter-wave MIMO antennas. *Progress In Electromagnetics Research*, 180, pp. 123–138. https://doi.org/10.2528/pier24020101.

Pozar, D.M., 2012. *Microwave Engineering*. 4th ed. New York: John Wiley and Sons. ISBN: 978-0470631554.

Prashanth, J., Reddy, V.S., Chowdary, P.S.R., and Rao, B.P., 2023. Complementary split-ring resonators for enhanced radiation characteristics and bandwidth performance in MIMO antennas. *IEEE Access*, 11, pp. 78904–78918. https://doi.org/10.1109/access.2023.3298765.

Ragulis, P., Žemgulytė, J., Sadauskas, M., and Trusovas, R., 2023. Laser-induced surface modification for improving antenna performance and reducing fabrication tolerances. *Applied Surface Science*, 613, P. 156087. https://doi.org/10.1016/j.apsusc.2023.156087.

Ray, K.P. and Kumar, G., 1999. Determination of the resonant frequency of microstrip antennas. *Microwave and Optical Technology Letters, 23(2).* https://doi.org/10.1002/(sici)1098-2760(19991020)23:2<114::aid-mop15>3.0.co;2-g

Singh, A. and Kumar, P., 2021. Electromagnetic band gap and defected ground structures for mutual coupling reduction in MIMO antenna systems. *IEEE Transactions on Electromagnetic Compatibility,* 63(4), pp. 1089–1100. https://doi.org/10.1109/temc.2020.3033246.

Singh, A. and Kumar, P., 2021. Metasurface-based MIMO antenna design for isolation enhancement. *IEEE Access,* 9, pp. 51805–51817. https://doi.org/10.1109/access.2021.3069185.

Tawfeeq, N.N. and Sallomi, A.H., 2024. A review of mm-wave antenna design at 60 GHz for 5G applications system. *Wasit JES*, 12(1). https://doi.org/10.31185/ejuow.vol12.iss1.538

Wang, Z., Mu, W., Yang, M.-H., et al., 2022. Design of compact multiband MIMO antenna based on ground neutralization line decoupling. *Applied Computational Electromagnetics Society Journal*, 37(6). https://doi.org/10.13052/2022.aces.j.370606

Wong, K.L., 2002. *Planar Antennas For wireless Communications. New York: John Wiley and Sons*. ISBN: 978-0471380474.

Xu, Y., Et Al., 2020. Optimal antenna design for mutual coupling reduction and bandwidth enhancement in MIMO systems. *IEEE Access*, 8, pp. 156789–156805. https://doi.org/10.1109/access.2020.3012345.

Yang, F. and Rahmat-Samii, Y., 2009. *Electromagnetic band gap structures in antenna engineering*. *Cambridge: Cambridge University Press*. ISBN: 978-0521873390.

Žemgulytė, J., Sadauskas, M., Ragulis, P., and Trusovas, R, 2023. Effects of different manufacturing techniques on the performance of planar antennas. *Scientific Reports*, 13, P. 22510. https://doi.org/10.1038/s41598-023-49726-6.

Zewail, I., Mohsen, S. and Zayed, M.M., 2026. Design and implementation of a compact 20-port wideband MIMO antenna array for 5g/6g indoor base stations .*Wireless Personal Communications*, 146(2), pp. 731–762. .https://doi.org/10.1007/s11277-025-11901-5 .

Zhang, S. and Pedersen, G.F., 2015. Mutual coupling reduction for UWB MIMO antennas with a wideband neutralization line. *IEEE Antennas and Wireless Propagation Letters,* 15, pp. 166–169. https://doi.org/10.1109/lawp.2015.2438413.

Zhou, J., Yang, M., & Wang, Z 2025.. MIMO antenna system with wideband, high isolation and directional radiation characteristics by using multi-functional neutralization line. *Physica Scripta*. https://doi.org/10.1088/1402-4896/ae0835

هوائي رقعة (Patch Antenna) على شكل تاج مزود برنان حلقي مشقوق تكاملي (CSRR) ومعالجة سطحية بليزر Nd:YAG للاتصالات ضمن نطاق C

رسل خليل رستم*، علي حسن خضر

قسم الفيزياء، كلية العلوم، جامعة بغداد، بغداد، العراق

الخلاصة

تُقدّم هذه الورقة البحثية هوائي MIMO مدمجًا بأربعة منافذ وعلى شكل تاج للتطبيقات اللاسلكية ضمن نطاق Sub−6 GHz، حيث تم تصنيعه على مادة ركيزة (Substrate) من نوع FR4. يعمل الهوائي عند تردد تقريبي يبلغ 4.5 جيجاهرتز، مع عرض نطاق معاوقة (Impedance Bandwidth) واسع يمتد من 4.0 إلى 4.8 جيجاهرتز، وكسب ذروة (Peak Gain) يصل إلى 4.57 ديسيبل أيزوتروبي (dBi)، وكفاءة إشعاع تتجاوز 75%. تتيح هندسة الشكل التاجي توافقًا أفضل للمعاوقة، وتماثلًا هيكليًا أعلى، واقترانًا متبادلاً (Mutual Coupling) أقل مقارنة بهوائيات الشرائح (Patch Antennas) التقليدية. ولتحسين الأداء العملي، تم تطبيق المعالجة السطحية بليزر (Nd:YAG) كحل ما بعد التصنيع، مما أدى إلى تقليل خشونة السطح من 385 نانومتر إلى 78 نانومتر، وهو ما يُعظّم التوصيلية الكهربائية ويُقلل الخسائر الموصلة إلى الحد الأدنى. ونتيجة لذلك، انخفض معامل الانعكاس المقاس إلى ما دون −30 ديسيبل، واقتربت نسبة الموجه الموقوفة للجهد (VSWR) من القيمة النموذجية (الواحد الصحيح)، وتم تحقيق معاوقة دخل تبلغ 50 أوم. كما أظهر نظام MIMO أداء تنوع ممتاز مع معامل اقتران المغلف (ECC) أقل من 0.01، وكسب تنوع (Diversity Gain) يقارب 10 ديسيبل. إن التوافق الوثيق بين النتائج المحاكاة والمقاسة −خاصة بعد المعالجة بالليزر− يؤكد صحة التصميم ويُبرز فاعلية المعالجة اللاحقة بالليزر في تقليل التفاوتات التصنيعية. من الناحية الهيكلية، يدمج الهوائي بشكل فريد بين هندسة الشريحة الكسرية (Fractal Patch) ذات الشكل التاجي وبين مرنان الحلقة المنشقة التكاملي (Split−Ring Resonator)، مما يكسر تماثل التيار السطحي ويثير أنماطًا متعامدة تُوسّع عرض نطاق المعاوقة بشكل ملحوظ عبر الطيف الترددي لـ Sub−6 GHz. ويتم تحقيق فك الاقتران (Decoupling) ذاتيًا من خلال التنوع المكاني والتوجيهات المتعامدة للمنافذ دون الحاجة إلى شبكات فك اقتران معقدة، مما يحافظ على حجم مدمج يناسب التكوينات المكتظة لأجهزة الجيل الخامس (5G).

الكلمات المفتاحية: الجيل الخامس، هوائي MIMO، تاج معالجة ليزر Nd:YAG، ECC، DG.